IL NUOVO CIMENTO Vol. 25 C, N. 5-6 Settembre-Dicembre 2002

Dynamics of the solar photosphere: THEMIS observations(*)(**)

F. Berrilli(1), G. Consolini(2) and E. Pietropaolo(3)

(1) *Dipartimento di Fisica, Università di Roma "Tor Vergata" - I-00133 Rome, Italy*

(2) *CNR, Istituto di Fisica dello Spazio Interplanetario - I-00133 Rome, Italy*

(3) *Dipartimento di Fisica, Università di L'Aquila - I-67100 L'Aquila, Italy*

(ricevuto il 10 Giugno 2002; approvato il 7 Agosto 2002)

Summary. — We present the results of 2D narrow- and broad-band photometry of quiet granulation field as observed at the center of the Sun by the THEMIS telescope in IPM mode. The broad-band spectral images have been used to derive geometrical and statistical properties of the pattern produced by convective flows rising from deep layers of the Sun. The narrow-band spectral observations, in the C I 538.0 nm, Fe I 537.9 nm, and Fe I 557.6 nm photospheric lines, have been used to calculate velocity and intensity maps at different heights in the solar atmosphere. The autocorrelation functions of the velocity fields at different heights suggest that, near the solar surface, the dynamics resemble the behavior of a complex out-of-equilibrium system, characterized by a dynamical heterogeneity. Conversely, in the middle photosphere, where only one characteristic time exists, the dynamical heterogeneity disappears. Moreover, the characteristic scales, derived from photospheric velocity maps by means of wavelet and information entropy analysis, show a dependence of their properties on the formation height of photospheric lines and an enlargement of the velocity features with height.

PACS 96.60.Mz – Photosphere, granulation.
PACS 01.30.Cc – Conference proceedings.

1. – Introduction

Nowadays, thanks to the availability of high-quality observational data from ground and space, complete spectral information begins to be available over a wide range of scales

(*) Paper presented at the International Meeting on THEMIS and the New Frontiers of Solar Atmosphere Dynamics, Rome, Italy, March 19-21, 2001.
(**) Based on observations made with THEMIS operated on the island of Tenerife by CNRS-CNR in the Spanish Observatorio del Teide of the Instituto de Astrofìsica de Canarias.

from the whole Sun down to the sub-granulation. Particularly, high spatial and spectral resolution observations of the solar surface allow the investigation of the convective pattern emerging in the photosphere. The description of dynamics of the atmospheric layers, where convective motions brake, and the association with the geometry of the observed structures, have profound implications on a variety of topics, ranging from energy transport in astrophysical plasmas to physics of fluids at high Reynolds numbers. Moreover, the solar convection represents the main test bench for stellar modeling, being the only example of astrophysical convection that can be directly investigated.

In the last decade many studies focused on the investigation of solar convection and, especially, on the possible relevance of turbulence for the understanding of solar granulation dynamics. Anyway, solar convection represents a very complex phenomenon, involving non-linear interactions as well as non-local chaotic processes. In this framework the study of solar convective patterns will benefit of the new concepts and analytical tools developed to characterize the dynamics of complex and drive out-of-equilibrium systems. Previous analyses of the photospheric velocity and intensity patterns evidence the existence of scaling features and intermittency in the dynamics of solar granulation [1-3].

Here, using broad-band and monochromatic images, we investigate the statistical features of granulation pattern and convection structures as well as the braking of the matter flows in the deepest layers of the photosphere.

2. – Observations and data processing

The present analysis uses different time series of broad-band (4 nm FWHM around 557 nm) and narrow-band (2.1 pm FWHM) pictures acquired on 1999, July 1 (from 7:21 to 8:24 UT). Observations were carried at the THEMIS telescope (Observatorio del Teide, Tenerife) with the IPM observing mode. The IPM mode consists in a Universal Birefringent Filter followed by a Fabry-Pérot interferometer [4]. A square portion ($34'' \times 34''$) of the quiet disk center was imaged with the broad-band CCD camera and, simultaneously, with the narrow-band CCD camera at different spectral points along the profile of C I 538.03 nm ($\Delta\lambda = 0, \pm 4, \pm 6$ pm, continuum), Fe I 537.9 nm ($\Delta\lambda = 0, \pm 4, \pm 6$ pm), and Fe I 557.61 nm ($\Delta\lambda = 0, \pm 6, \pm 8, \pm 10$ pm, continuum) lines. Each spectral series consisted of 19 broad-band and 19 narrow-band images. We used two different integration times, 40 ms and 200 ms, for broad-band and narrow-band frames, respectively. The two 12-bit CCD cameras [5] are binned to 256×256 for a final image scale of $0.134''$/pixel. Seeing conditions and telescope set-up limited the spatial resolution to 0.3–$0.5''$ for broad-band images. The time interval between two successive images and two successive spectral series was 2.5 s and 75 s, respectively.

After the standard correction of the images for dark current, flat field, image motion, and tracking loss of the telescope, the final dimension of the images was restricted to a sub-array of $\sim 30'' \times 30''$. The selected 40-minutes sequence used for the final analysis consists of 32 spectral series for a total of 608 broad-band and 608 narrow-band frames. To reduce the noise and take into account the instrumental profile, we applied a Wiener filter [6] to broad-band images. We assumed a Gaussian point spread function (FWHM = $0.4''$, comparable with the spatial resolution of the broad-band observations) and a S/N ratio equal to 15, which was found to represent a good compromise between the level of restoration and the noise amplification. In fig. 1 we reported a typical image after the application of the Wiener filter.

In the IPM observing mode, narrow-band images, corresponding to a single line profile, were acquired one wavelength position at a time; therefore, to derive physical quanti-

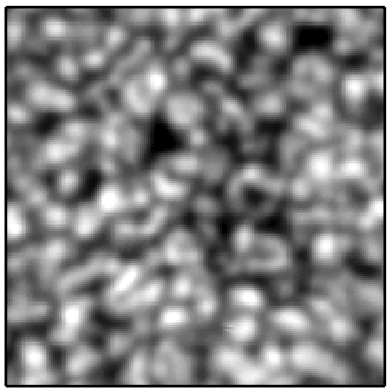

Fig. 1. – Wiener restored (FWHM = 0.4″, S/N = 15) image, with contrast equal to 7.9%. The box size is 30″ × 30″. The original image, with contrast equal to 4.9%, was obtained, with an integration time of 40 ms at 557.6 nm by a 4 nm passband, at THEMIS telescope in IPM observing mode.

ties like the Doppler velocity [1,7], we used for each spectral series a Fourier interpolation to shift in time the observations to the same instant.

The average photospheric heigth of C I 538.0 nm, Fe I 537.9 nm, and Fe I 557.6 nm lines are, respectively, 0 km, 120 km, and 110 km, as evaluated on the basis of their velocity response function [8].

Solar features have been identified with a numerical procedure [9,10] that consists of two different steps. The first step is based on an iterative MAT (Medial Axis Transform) procedure that extracts reticular structures. In our images reticular intensity structures represent intergranular lanes, while reticular velocity structures represent downflow lanes. Intensity and velocity reticular structures identify the boundaries of granular and convective cells, respectively.

The second step is based on a dynamical threshold and extracts compact structures. Granules are extracted from intensity images, while upflow regions are extracted from velocity maps. The dynamical threshold value depends on the pixel position and on the statistical properties of a suitable moving box [11]. We used a 3″ × 3″ box centered on the selected pixel. A successive segmentation algorithm, based on a region growing by pixel aggregation, calculates statistical and geometrical information from identified structures.

3. – Intensity distribution and time evolution of velocity fields

The intensity distribution, as obtained from a broad-band image, is reported in fig. 2. The observed intensity of the emergent radiation shows an asymmetric shape that is in agreement with Stein and Nordlund simulations [12] smoothed to model the actual observations. The observed asymmetry derives from a bimodal distribution of the emergent intensity in which dark, connected, intergranular lanes give a more significant contribution than bright granules.

Besides intensity fluctuations, a relevant parameter used to characterize the photospheric pattern is the lifetime of the observed structures. In order to study the temporal evolution of the velocity fields, we investigate the time series of photospheric velocities

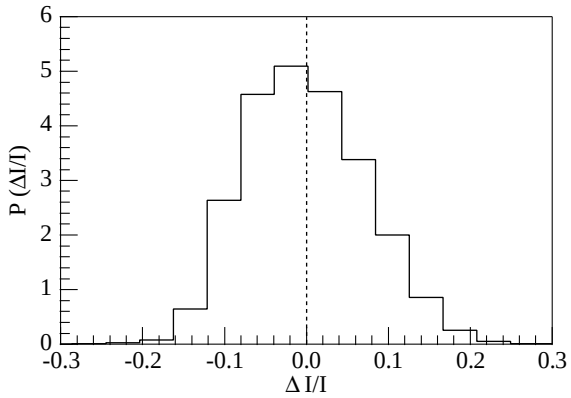

Fig. 2. – Probability density function of emergent intensity as obtained from a broad-band image at 557.6 nm.

relative to the same photospheric line. In detail, we evaluated the temporal autocorrelation function TAC (τ) for the 12 successive velocity patterns (about 15 minutes). For each line we obtained a total of 24 TAC (τ) trends that are averaged and plotted in fig. 3. In the case of the C I line the autocorrelation function has been fitted by a stretched exponential decay function, whose form is the following:

$$C(\tau) \propto \exp\left[-\left(\frac{\tau}{\tau_0}\right)^{\beta}\right] \tag{1}$$

with $\tau_0 = [133 \pm 6]$ s and $\beta = [0.46 \pm 0.02]$. The stretched exponential provides a good representation of experimental and numerical data in a wide variety of complex and out-of-equilibrium systems [13]. Conversely, in the case of Fe I data the TAC is given by a simple exponential fit with characteristic times $\tau_0 = [367 \pm 4$ s$] \sim 6$ min, and $\tau_0 = [417 \pm 6$ s$] \sim 7$ min for Fe I 537.9 nm and Fe I 557.6 nm line, respectively. The existence of a stretched exponential function in the case of C I velocity field should be read as evidence of dynamical heterogeneity in the temporal evolution of the velocity structures. This is to say that the evolution of the velocity structures is not dominated by a single characteristic time, but, conversely, is the results of a complex dynamics involving many competing structures characterized by a hierarchy of lifetimes. This aspect will be discussed in detail elsewhere.

4. – Multiresolution analysis: the characteristic scales of the velocity field

The multiresolution analysis method, directly related to the theory of wavelets and filter banks, employs wavelets as high-pass linear filters and an additional set of complementary functions, known as scaling functions, which take effect of low-pass linear filters. This method was previously applied to the study of the characteristic chromospheric spatial scales by the full disk observations of Ca-II K line at PSPT-OAR telescope [10]. The method, valid for 1D functions, could be extended to 2D frames by using a combination of 1D wavelets, $\psi(x)$, and scaling functions, $\phi(x)$. The result is a scaling function $\Phi(x, y)$ and three wavelet functions, $\Psi^{\mathrm{h}}(x, y)$, $\Psi^{\mathrm{v}}(x, y)$ and $\Psi^{\mathrm{d}}(x, y)$, one for each elementary di-

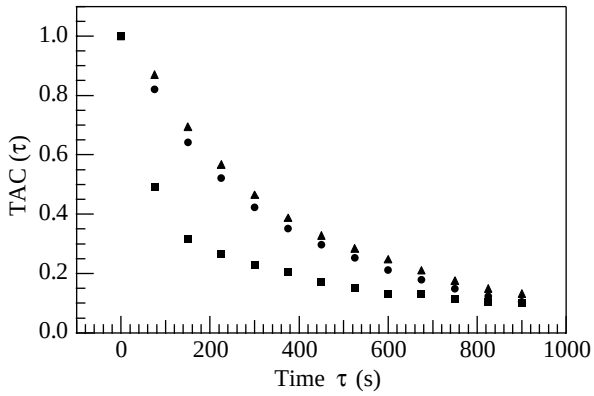

Fig. 3. – Average temporal autocorrelation function TAC (τ) for the time evolution of the velocity fields as observed with the three spectral lines. Solid squares, dots and triangles refer to C-I 538.0 nm, Fe-I 537.9 nm and Fe-I 557.6 nm spectral lines, respectively.

rection of application (h,v, and d stand for horizontal, vertical, and diagonal direction). In this analysis we use Haar wavelets. When applied to a broad-band image, the method produces the results shown in fig. 4, where the sub-images (see fig. 4 on the right) are the set of wavelet coefficients for each of the considered scales.

We use the set of wavelet coefficients to define the energy spectrum of a single image:

$$E^{\mathrm{s}}(j) = \sum_{i=1}^{N_{\mathrm{coef}}} \mid f_i^{\mathrm{s}}(j) \mid^2 , \tag{2}$$

where $f_i^{\mathrm{s}}(j)$ are the wavelet coefficients at a given position i and scale j for the three directions s $\in$ [h, v, d]. As previously shown in the case of chromospheric structures [10] and for granulation patterns [14], the average energy spectra, when plotted *vs.* the scale j, peaks at the characteristic scales of the observed structures. For example, in the case

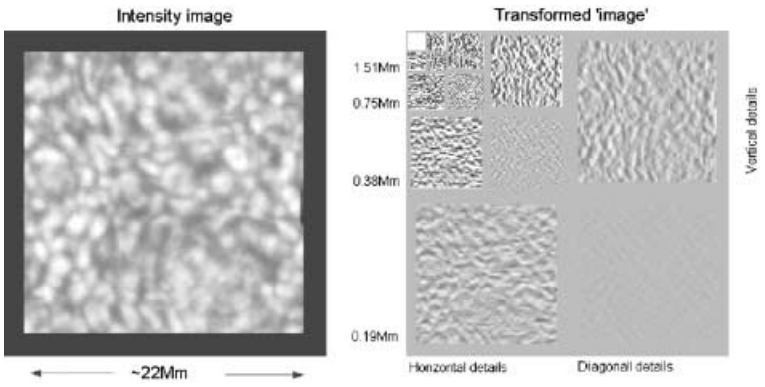

Fig. 4. – Left: original image padded with zeros to fit the nearest power of 2 for the linear dimensions. Right: the same image as represented in the wavelet domain by means of the multiresolution analysis and ordered by analyzed scale and direction.

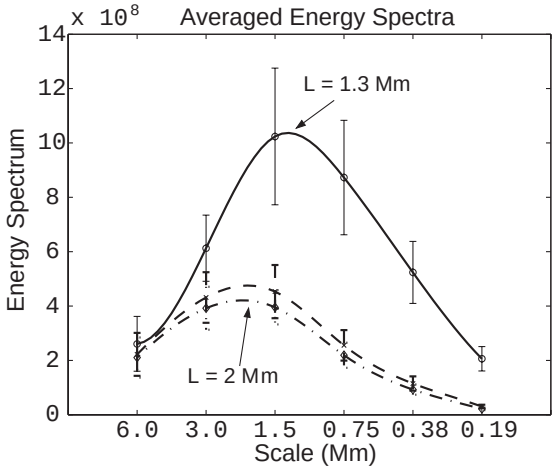

Fig. 5. – The analysis applied on three different sets of velocity maps,C I 538.0 nm, Fe I 537.9 nm, and Fe I 557.6 nm photospheric lines, represents three different photospheric heights.

of granulation patterns it is possible to observe an excess of energy at $L \simeq 1.2$ Mm. This analysis has been applied to the three different sets of velocity maps representing three different photospheric heights, as previously mentioned in sect. **2**. Figure 5 shows the obtained results. Here, solid curves correspond to spline interpolations.

The present analysis of velocity characteristic scales shows evidence of a variation of velocity field structural properties with photospheric height. In detail, we found a broadening of velocity structures with the height. This result is in good agreement with the previous findings of the sign-singularity analysis of velocity fields [1], where the cutoff scale was found to increase with photospheric height.

5. – Information entropy and solar photospheric structures

One of the key points of the photospheric velocity and intensity pattern studies is the analysis of the relevant scales over which morphological structures are present.

A different way to investigate the existence of relevant scales at the solar photosphere could be that of making use of the "information theory" to study the morphology of photospheric structures. Recently, Van Siclen [15] introduced a very general normalized measure of the "information entropy" to characterize the emergent microstructures in the case of a population of interacting particles. Van Siclen's normalized information entropy measure H is defined as the difference between the information entropy of a perfectly random spatial distribution and that of a clustered configuration, *i.e.*

$$H(r) = H(r) - H_{\mathrm{R}}(r)\,, \tag{3}$$

where $H(r)$ is the information entropy of the clustered configuration

$$H(r) = -\sum_i P_i(r) \log[p_i(r)] \tag{4}$$

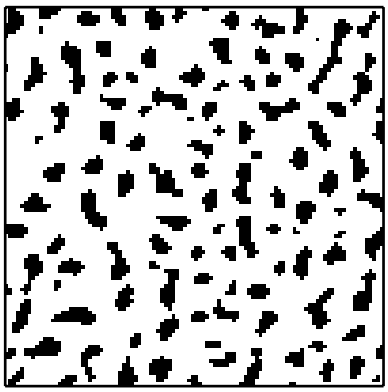

Fig. 6. – Example of binarized (two-levels) frame obtained from a C I 538.0 nm velocity map.

and $H_{\mathrm{R}}(r)$ is the reference information entropy for a completely random distribution,

$$H_{\mathrm{R}}(r) = -\sum_i p_i(r) \log[p_i(r)]\,, \tag{5}$$

where p_i and P_i are the expected and actual probability of finding i particles in a surface box of dimension $r \times r$. The maxima of the normalized information entropy are correlated with those length scales at which the distribution of particles differs the most from a random configuration. Conversely, the minima refer to those length scales at which the system is periodic.

We applied such analysis to binary images of velocity fields (see previous sections for more details) where each black pixel has been associated with a particle, following the idea of Van Siclen. Figure 6 shows an example of such binary velocity fields. The results of this analysis are briefly summarized in fig. 7, where we report the average normalized

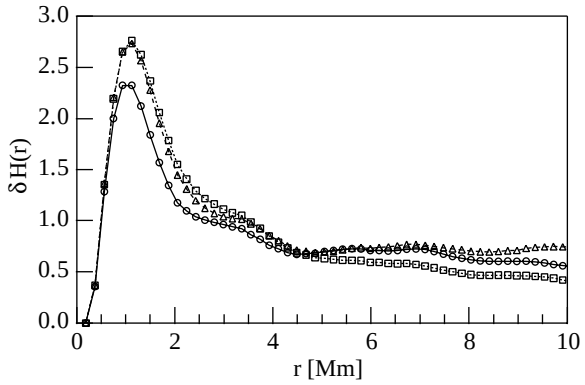

Fig. 7. – The analysis applied on three different sets of velocity maps, C I 538.0 nm, Fe I 537.9 nm, and Fe I 557.6 nm photospheric lines, representing three different photospheric heights. Open circles refer to C I 538.0 nm data, while open triangles and squares refer to Fe I 537.9 nm and Fe I 557.6 nm data, respectively.

information entropy at the three photospheric heights, here investigated, as resulting from the complete sets of velocity fields. The first maximum appears to be located in the range from 1.0 to 1.5 Mm and must be connected with the scales related to granular convection cells. A clear dependence of the typical length scale of such first maximum upon the photospheric height is found, indicating an evolution of the structures. As underlined by Van Siclen [15], the secondary maxima in fig. 7 could be associated with the cluster of convective cells, perhaps related with other characteristic scales in the velocity fields. For example, a less evident second maximum is found in the range from 2.5 Mm to 4 Mm, a scale generally associated to mesogranular flows that could involve the clusterization of convective cells. However, we remark that at this stage a precise association of these secondary maxima with different photospheric structures requires further and more accurate analyses, that will be presented elsewhere.

* * *

We thank B. Caccin and V. Penza for the calculation of RF curves, C. Giammanco for the $k-\omega$ filter, and F. Lepreti for the time shift correction of narrow-band images. We also thank the THEMIS staff for the efficient support in the observations.

REFERENCES

[1] Consolini G., Carbone V., Berrilli F. *et al.*, *Astron. Astrophys.*, **344** (1999) L33.
[2] Lepreti F., Carbone V., Pietropaolo E., Consolini G., Bruno R., Bavassano R. and Berrilli F., *Physica A*, **280** (2000) 88.
[3] Berrilli F., Consolini G., Pietropaolo E., Caccin B., Penza V. and Lepreti F., *Astron. Astrophys.*, **381** (2001) 253.
[4] Cavallini F., *Astron. Astrophys. Suppl.*, **128** (1998) 589.
[5] Berrilli F., Caccin B., Cantarano S. and Egidi A., *Nuovo Cimento*, **20** (1997) 297.
[6] Hunt B. R., *Image Restoration in Digital Image Processing Techniques* (Academic Press, Inc.) 1984.
[7] Berrilli F., Florio A., Consolini G. *et al.*, *Astron. Astrophys.*, **344** (1999) L29.
[8] Caccin B., Gomez M. T., Marmolino C. and Severino G., *Astron. Astrophys.*, **54** (1977) 227.
[9] Florio A. and Berrilli F., *Mem. SAIt*, **69** (1998) 655.
[10] Berrilli F., Ermolli I., Florio A. and Pietropaolo E., *Astron. Astrophys.*, **344** (1999) 965.
[11] Gonzalez R. C. and Wints P., *Digital Image Processing* (Addison-Wesley Publishing Company) 1987.
[12] Stein R. F. and Nordlund A., *Astrophys. J.*, **499** (1998) 914.
[13] Careri G. *et al.*, *Phys. Rev. E*, **64** (2001) 052901.
[14] Pietropaolo E., Berrilli F., Consolini G., Smaldone L. A., Straus T., Cauzzi G., Bruno R. and Bavassano B., *ESA SP*, **448** (1999) 343.
[15] Van Siclen C. DeW., *Phys. Rev. E*, **56** (1997) 5211.